Article

JOURNAL OF THE CHINESE CHEMICAL SOCIETY

Theoretical Study on the Gas-Phase S_N2 Reaction of Microhydrated Fluoride with Methyl Fluoride

Jien-Lian Chen and Wei-Ping Hu*

Department of Chemistry and Biochemistry, National Chung Cheng University, Chia-Yi 621, Taiwan

(Received: Mar. 7, 2012; Accepted: May 28, 2012; Published Online: Jun. 28, 2012; DOI: 10.1002/jccs.201200128)

The rate constants for the gas-phase S_N2 reaction of $F^-(H_2O)$ with CH_3F have been calculated using the dual-level variational transition state theory including multidimensional tunneling from 50 to 500 K. Tunneling was found to dominate the reaction below 200 K. The deuterium, ^{13}C, and ^{14}C kinetic isotope effects (KIEs) and solvent (D_2O) isotope effects (SKIEs) were also calculated in the same temperature range. The results indicated that the deuterium and heavy water substitutions resulted in inverse KIEs (0.6~0.8) while the ^{13}C and ^{14}C substitutions resulted in normal KIEs (1.0~1.2) at room temperature. The calculated carbon KIEs increased significantly below 80 K due to the differences in the magnitude of the tunneling effects for different isotopic substitutions.

Keywords: S_N2 reaction; Microsolvation; Dual-level dynamics; Variational transition state theory; Tunneling effects; Kinetic isotope effects; Solvent kinetic isotope effects.

INTRODUCTION

The bimolecular nucleophilic substitution (S_N2) reaction is one of the most studied reactions in organic chemistry and it plays very important roles in organic synthesis.[1-12] Measurement of the kinetic isotope effects (KIEs) have proved to be very useful for investigating the reaction mechanisms. For example, alkyl halides and a nucleophilic group can undergo E2 or S_N2 pathway, and the observed deuterium KIEs could differentiate between these pathways. The E2 reaction would show high deuterium KIEs at room temperature (k_H/k_D = 2-6)[4-7,13] while the S_N2 reaction usually would show slightly inverse KIEs (k_H/k_D = 0.8-1.0).[4-7] Experimental and theoretical studies on many simple gas-phase S_N2 reactions have been reported.[4-12] For example, the deuterium KIEs for the $Cl^- + CH_3Br$ reaction have been experimentally determined to be 0.80[4] and 0.88,[8] while the theoretical prediction gave a higher value of 0.94 at 298 K.[11] The experimental deuterium KIE for the $Cl^- + CH_3I$ reactions was found to be 0.84[4] and a theoretical study predicted a value of 0.91.[11] The experimental deuterium KIE for the $Br^- + CH_3I$ reactions was 0.76,[4] while the predicted value was 0.93.[11] The experimental deuterium KIE for the $F^- + CH_3Cl$ was found to be 0.90,[10] and a theoretical study predicted a value of 0.92.[9] The microsolvated reaction (solvation by one or a few solvent molecules) is a previously missing link between gas phase and solution kinetics.[10,14-17] The study of microsolvated systems both experimentally and theoretically allows us to understand the direct solvation effects on the first solvation shell at detailed molecular level. In addition, introducing strong solvation effects on the ionic species in the gas-phase S_N2 or E2 reactions usually increases the reaction energy barriers significantly. This in turn makes the comparison between the experimental results and transition state theory prediction much more meaningful. Due to the much higher energy barriers in the solvated reactions the reaction bottleneck is located close to the transition state, and the reaction can be modeled more accurately by the transition state theory. While in many unsolvated systems, due to the very small or negligible energy barriers, the reaction rates are sometimes very close to the collision rates. We have previously studied the microhydrated S_N2 reaction of $F^-(H_2O) + CH_3Cl$.[14] The calculated inverse KIEs from the CD_3 and D_2O substitutions at 300 K were 0.83 and 0.65, respectively, which were in very good agreement with experimental values.[10] The theoretical studies of the S_N2 reactions $Cl^-(H_2O)_n + CH_3Cl$ (where n = 0-2) have also been reported.[15] The predicted barrier heights by MP2/6-31G** method were 3.0, 5.4 and 10.7 kcal/mol for n = 0,1, and 2, respectively. The predicted KIEs due to the CD_3 substitutions were 0.95, 0.94 and 0.91 for n = 0, 1, and 2, respectively. The experimental studies of $F^-(H_2O) + CH_3Br$ have also been reported.[10,16] The measured KIEs due to the CD_3 and D_2O substitutions at 300 K were 0.92 and 0.83,[10] respectively, while the computational results were 0.84 and 0.65,[16] respectively. In addition, the experimental KIE for

* Corresponding author. E-mail: chewph@ccu.edu.tw

the $OH^-(H_2O)$ + CH_3Br reactions due to the CD_3 substitution was found to be 0.98 at 300 K.[17] However, most of the gas-phase S_N2 reactions experimentally studied so far have low energy barriers, and thus the tunneling effects can be safely ignored. However, due to the formation of ion-dipole complexes, the S_N2 reactions usually have relatively narrow barriers. In principle, the tunneling effects could be important at lower temperature due to the motion of hydrogen and carbon atoms if there is a positive energy barrier. The study of the S_N2 reaction of $F^-(H_2O)$ + CH_3F (R1), which has a small positive barrier height and involves the lightest halogen, offer a good opportunity to study the tunneling effects on the rate constants, and various kinetic isotope effects. Thus, in the current study, we applied the variational transition state theory including multidimensional tunneling (VTST/MT)[18-21] corrections to calculate the thermal rate constants of R1 and various isotopically substituted analogs over a wide temperature range. The temperature dependencies of the rate constants, tunneling effects, and kinetic isotope effects were calculated and discussed.

COMPUTATIONAL METHODS

The molecular geometry and harmonic vibrational frequencies of the stationary points were calculated using MP2[22] and B3LYP[23] theory with the aug-cc-pVDZ and aug-cc-pVTZ[24] atomic basis sets. Single-point energies at the stationary points were calculated with the CCSD(T)[25] theory with the aug-cc-pVTZ basis set. Dual-level[26] VTST/MT dynamics calculation was performed to obtain the thermal reaction rate constants over the temperature range of 50 K to 500 K. The low-level reaction path information was calculated using the MP2/aug-cc-pVDZ method as required for the VTST/MT calculation. The reaction path was calculated from –3.6 to 3.9 bohrs with a gradient step size of 0.006 bohr and a hessian step size of 0.03 bohr using the Page-McIver method[27] in the mass-scaled coordinates with a scaling mass of 1 amu. The hessians are the force constant matrices which served two purposes. The first one is to provide the necessary second derivatives as required by the Page-McIver method for reaction-path following. The second is to obtain, after projecting out the reaction path direction, the vibrational eigenvectors and eigenvalues along the reaction path. Cartesian coordinates were used to calculate the vibrational frequencies of the generalized transition states along the reaction path. The dual-level VTST also requires a set of "high-level" energy data on the stationary points along the reaction path for the interpolated corrections to the low-level PES. These energies data were obtained at the CCSD(T)/aug-cc-pVTZ level. The SIL-1 interpolated correction scheme[28] was applied in the dual-level calculation using the CCSD(T)/aug-cc-pVTZ energies along the low-level reaction path geometries to estimate the barrier widths. The rate constants as a function of temperature were calculated at the levels of conventional transition-state theory (TST), canonical variational theory (CVT),[18] and canonical variational theory with small-curvature tunneling approximation (CVT/SCT).[20] The small curvature tunneling (SCT) method is used here because it takes the reaction-path curvature into account, and this usually predicts a more favorable tunneling path. The SCT method has also been shown to give better results as compared to accurate quantum scattering calculation.[18-20] Rate constants of four other isotopically substituted analogs of R1, $F^-(H_2O)$ + CD_3F (R2), $F^-(D_2O)$ + CH_3F (R3), $F^-(H_2O)$ + $^{13}CH_3F$ (R4), and $F^-(H_2O)$ + $^{14}CH_3F$ (R5), have also been similarly calculated. The rotation symmetry number of CH_3F or CD_3F (C_{3v}) is three. Since the transition state structure (C_1) is chiral, the overall symmetry numbers of reaction were set to six. The electronic structure calculation was performed using the Gaussian 03 programs,[29] and the dual-level VTST/MT calculation was performed using the Gaussrate 8.2 program[30] which is an interface between the Gaussian 03 and POLYRATE 8.2 program.[31]

RESULTS AND DISCUSSION

(a) Energetics and Geometry

Table 1 shows the calculated barriers and the energies of reaction at various theoretical levels. The products could in principle be (a) CH_3F + $F^-(H_2O)$ (b) $CH_3F^-(H_2O)$ + F^- (c) CH_3F + F^- + H_2O. The products of the (a) channel is identical to the reactants, and thus channel (a) is isoergic. The predicted reaction energies for channels (b) and (c) were 23.5 kcal/mol and 27.8 kcal/mol at CCSD(T)/aug-cc-pVTZ level, respectively. The branching ratios depend on the detailed energy redistribution after passing the reaction bottleneck, and the forward rates to a good approximation are not affected by the branching ratios. Of course, in future experimental study, isotopic substitutions on fluorine would be required to deduce the absolute forward rates since the same ion, $F^-(H_2O)$ could appear both on the reactants and the products. The MP2/aug-cc-pVDZ and MP2/aug-ccpVTZ methods predicted energy barriers of 8.7 and 11.6 kcal/mol, respectively. The B3LYP methods predicted

Table 1. Calculated Reaction Energetics[a] (in kcal/mol)

	$CH_3F(H_2O) + F^-$	$CH_3F + F^- + H_2O$	ion-dipole complex $F^-(H_2O)\cdots CH_3F$	barrier height
MP2/aug-cc-pVDZ	22.3	26.8	12.3	8.7
MP2/aug-cc-pVTZ	23.4	27.6	11.6	11.6
B3LYP/aug-cc-pVDZ	23.9	27.3	10.5	7.9
B3LYP/aug-cc-pVTZ	24.2	27.3	10.0	9.7
CCSD(T)/aug-cc-pVTZ[b]	23.5	27.8	12.1	10.5

[a] Relative to $CH_3F + F^-(H_2O)$
[b] Using MP2/aug-cc-pVTZ structures

slightly lower barriers using the same basis sets. The CCSD(T)/aug-cc-pVTZ method predicted a barrier height of 10.5 kcal/mol which should be most reliable. For comparison, the transition state (TS) energy of $CH_3F + F^-$ reaction was also calculated with the CCSD(T)/aug-cc-pVTZ method at the MP2/aug-cc-pVTZ geometry. The calculated barrier height was −1.1 kcal/mol, in good agreement with previous studies.[32,33] The barrier height in the microsolvated system was 11.6 kcal/mol higher because of the difference in the solvation effects. The microsolvation energy was calculated to be 27.8 kcal/mol at the reactant (F^-) and was 16.2 kcal/mol at the transition state. (The solvation energy of TS mentioned here was obtained using the structure of the microsolvated TS, and by subtracting the energy of the structure with the water molecule removed and the energy of a free water molecule from the energy of the microsolvated TS. Thus, no structural distortion energy was included.) The TS has a delocalized charge distribution and thus a lower solvation energy. The ion-dipole complex $F^-(H_2O)\cdots CH_3F$ on the reactant side was predicted 12.1 kcal/mol lower than the reactant at CCSD(T)/aug-cc-pVTZ level. The calculated geometries of the stationary points of R1 at the MP2/aug-cc-pVTZ level are depicted in Figure 1. From the reactant to the TS, the C-F bond is lengthened by 0.516 Å and the C-H bond is slightly shortened by ~0.02 Å. The distance between F anion and the hydrogen bonded hydrogen in H_2O was predicted to be 1.368 Å at reactant and 1.638 Å at TS. The O-H bond of H_2O pointing to the fluoride ion was shortened 0.074 Å from the reactant to TS due to the weakening of the hydrogen bonding. The C-$F^-(H_2O)$ bond of the TS was predicted to be 1.739 Å. In comparison to the TS of the unsolvated reaction, the C-F (H_2O) bond in the microsolvated system was lengthened by 0.088 Å and the C-F bond was shortened by 0.077 Å. The C-H bond distances were found to be less sensitive to microsolvation.

(b) Rate Constants

Figure 2 shows the dual-level corrected potential energy curves along the reaction paths of both the unsolvated and microsolvated reactions. Evidently, one of the most important effects of microsolvation was to elevate the energy barrier, which decreased the rate constants considerably (by 10 orders of magnitude at 300 K in the current system) and at the same time allowed important contribution to the rate constants by tunneling effects at low temperature. The microsolvated curve was not symmetric because at the TS

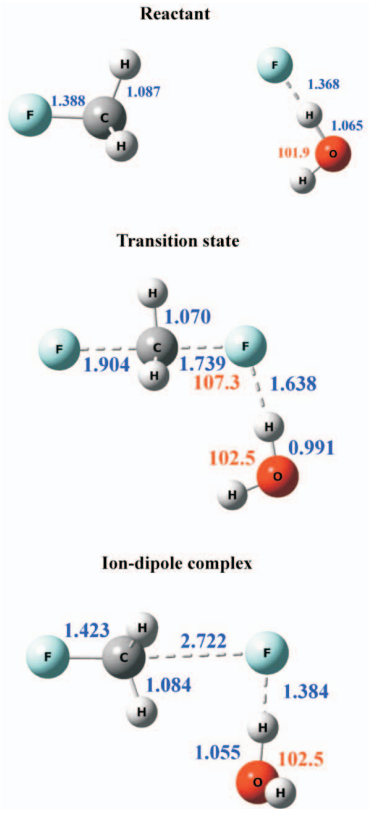

Fig. 1. Calculated structures by the MP2/aug-cc-pVTZ method. Bond lengths are in Å (blue) and bond angles in degrees (red).

the water molecule was still bound to the incoming fluoride ion, as shown in Figure 1, and has not yet moved to the outgoing fluoride ion.

The calculated rate constants from 50 K to 500 K are listed in Table 2, and the corresponding Arrhenius plots are shown in Figures 3 and 4. The variational effects[18] in the current systems were found to be very small at all temperatures and thus the TST and CVT results are almost identical (the CVT results are omitted). This is due to the relatively sharp barrier (with half-height width of ~1.2 bohrs) as seen in Figure 2. This sharp barrier also caused the important tunneling effects at low temperature. As seen in Table 2, the tunneling effects of all the reactions became dominant below 200 K and raised the rate constants dramatically at even lower temperature. This was also shown in the apparent curvatures in the Arrhenius plots of Figures 3 and 4. For example, the tunneling effects increase the TST rate constants of R1 by factors of 2.2×10^{15}, 1000, 5.6, and 2.2 at 50, 100, 150, and 200 K, respectively. Even at 300 K, tunneling is still important and increases the rate constant of R1 by 39%.

For gas-phase S_N2 reaction, the tunneling contribution to the rate constants in the current system is particularly large, considering the reaction path is dominated by heavy-atom motions. In contrast, as seen in Figure 2, the tunneling would not have any significant effects on the unsolvated reaction since the energy of the TS is below that of the reactants. It was the significant differences in solvation energies among the structures on the reaction path and the relatively narrow width of the energy barrier that made the important tunneling effects possible. We also checked the large curvature tunneling (LCT)[19-21] method and we found that the SCT is the dominant tunneling mechanism except at a very small lowest energy range. Inclusion of both the SCT and the LCT mechanisms (the μOMT method)[19] would only make negligible difference (< 5%) to the SCT results. The current result, to our knowledge, is the first accurate estimation of the tunneling contribution to the bimolecular rate constants of a gas-phase S_N2 reaction using a reliable, dual-level corrected potential energy surface

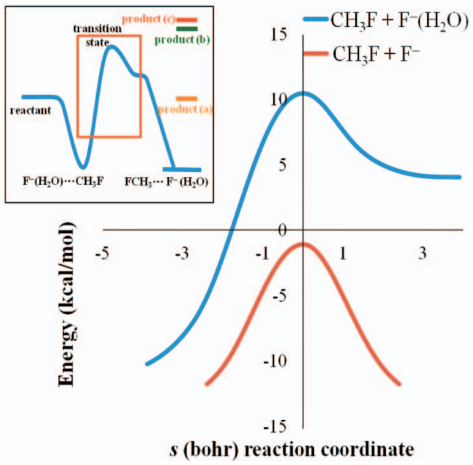

Fig. 2. The potential energy curves along the reaction paths of $CH_3F + F^-(H_2O)$ and $CH_3F + F^-$ reactions. The products (a), (b), and (c) in the schematic diagram on the upper left corner were $CH_3F + F^-(H_2O)$, $CH_3F(H_2O) + F^-$, and $CH_3F + F^- + H_2O$, respectively.

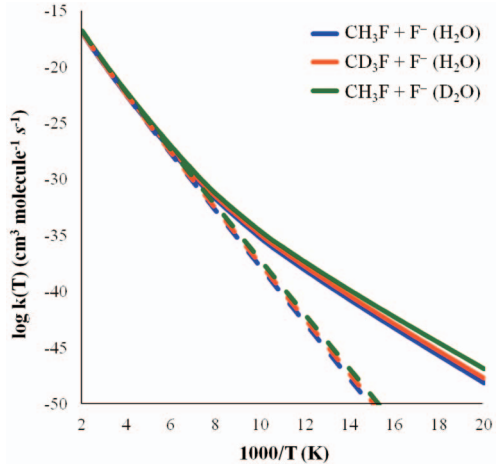

Fig. 3. The Arrhenius plot of the calculated rate constants. The broken and solid lines indicate results calculated at TST and CVT/SCT levels, respectively.

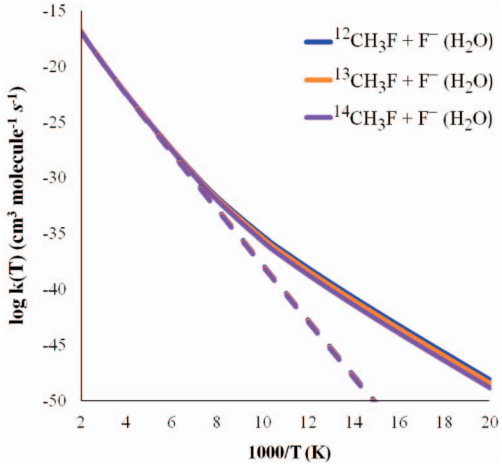

Fig. 4. The Arrhenius plot of the calculated rate constants. The broken and solid lines indicate results calculated at TST and CVT/SCT levels, respectively.

Table 2. Calculated Rate Constants (in cm^3 $molecule^{-1}$ s^{-1}) by the TST and CVT/SCT methods

T (K)	$CH_3F + F^-(H_2O)$		$CD_3F + F^-(H_2O)$		$CH_3F + F^-(D_2O)$		$^{13}CH_3F + F^-(H_2O)$		$^{14}CH_3F + F^-(H_2O)$	
	TST	CVT/SCT	TST	CVT/SCT	TST	CVT/SCT	TST	CVT/SCT	TST	CVT/SCT
50	6.73(–64)[a]	1.45(–48)	3.29(–63)	3.77(–48)	1.26(–62)	2.65(–47)	5.02(–64)	7.18(–49)	3.89(–64)	2.60(–49)
60	1.69(–55)	1.62(–44)	6.02(–55)	3.81(–44)	1.89(–54)	1.74(–43)	1.31(–55)	8.12(–45)	1.05(–55)	3.01(–45)
70	1.70(–49)	1.55(–41)	4.85(–49)	3.38(–41)	1.32(–48)	1.15(–40)	1.36(–49)	7.95(–42)	1.12(–49)	3.07(–42)
80	5.46(–45)	3.30(–39)	1.32(–44)	6.75(–39)	3.25(–44)	1.86(–38)	4.48(–45)	1.75(–39)	3.76(–45)	7.13(–40)
90	1.77(–41)	2.67(–37)	3.77(–41)	5.16(–37)	8.56(–41)	1.22(–36)	1.48(–41)	1.48(–37)	1.26(–41)	6.53(–38)
100	1.15(–38)	1.15(–35)	2.22(–38)	2.12(–35)	4.74(–38)	4.49(–35)	9.76(–39)	6.82(–36)	8.43(–39)	3.34(–36)
125	1.41(–33)	3.22(–32)	2.28(–33)	5.23(–32)	4.34(–33)	9.60(–32)	1.23(–33)	2.35(–32)	1.08(–33)	1.57(–32)
150	3.70(–30)	2.10(–29)	5.34(–30)	3.05(–29)	9.46(–30)	5.27(–29)	3.28(–30)	1.72(–29)	2.95(–30)	1.36(–29)
175	1.09(–27)	3.39(–27)	1.45(–27)	4.54(–27)	2.44(–27)	7.53(–27)	9.78(–28)	2.92(–27)	8.91(–28)	2.46(–27)
200	8.11(–26)	1.84(–25)	1.03(–25)	2.32(–25)	1.65(–25)	3.72(–25)	7.37(–26)	1.62(–25)	6.78(–26)	1.42(–25)
250	3.80(–23)	6.19(–23)	4.49(–23)	7.29(–23)	6.81(–23)	1.11(–22)	3.51(–23)	5.64(–23)	3.28(–23)	5.11(–23)
300	2.57(–21)	3.57(–21)	2.92(–21)	4.04(–21)	4.24(–21)	5.88(–21)	2.40(–21)	3.30(–21)	2.26(–21)	3.06(–21)
400	6.22(–19)	7.43(–19)	6.82(–19)	8.10(–19)	9.22(–19)	1.10(–18)	5.90(–19)	7.00(–19)	5.62(–19)	6.60(–19)
500	2.03(–17)	2.26(–17)	2.19(–17)	2.43(–17)	2.80(–17)	3.12(–17)	1.94(–17)	2.15(–17)	1.86(–17)	2.05(–17)

[a] 6.73(–64) means 6.73×10^{-64}

(PES). Non-negligible tunneling effects at and below room temperature in the gas-phase reaction of $Cl^-(H_2O) + CH_3Cl$ have also been predicted using VTST/MT but with an empirically adjusted analytical PES based on MP2/6-31G (d,p) calculations and experimental rate constants.[15]

(c) Kinetic Isotope Effects and Solvent Kinetic Isotope Effects

The calculated KIEs using the TST and CVT/SCT were shown in Table 3 and Figure 4. Here we defined the various KIEs as the ratios of the rate constants of the unsubstituted reaction (R1) to the rate constants of the various isotopically substituted reactions:

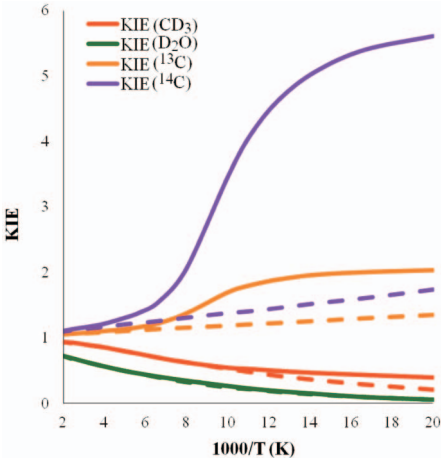

Fig. 5. Temperature dependence of the calculated KIEs. The broken and solid lines indicate results calculated at TST and CVT/SCT levels, respectively.

$$KIE(CD_3) = k(R1) / k(R2) \quad (1)$$

$$KIE(D_2O) = k(R1) / k(R3) \quad (2)$$

$$KIE(^{13}C) = k(R1) / k(R4) \quad (3)$$

$$KIE(^{14}C) = k(R1) / k(R5) \quad (4)$$

The calculated $KIE(CD_3)$ above 100 K by TST and CVT/SCT were very similar. The "inverse" deuterium KIE of 0.88 at 300 K by TST was in good agreement with previous studies on S_N2 reactions.[4-12] However, the calculated $KIE(CD_3)$ by the two methods became different at temperature below 100 K. Both methods predicted that $KIE(CD_3)$ would decrease (or more "inverse") as temperature decreases but the CVT/SCT method predicted a smaller temperature dependence. For example, at 100, 80, and 50 K the $KIE(CD_3)$ predicted by TST were 0.52, 0.41, and 0.20, respectively, while they were 0.54, 0.49, and 0.39 by CVT/SCT. Since the rate constants were dominated by tunneling at low temperature, the tunneling effects were stronger in the unsubstituted reaction as expected. The small tunneling effects on the calculated $KIE(CD_3)$ above 100 K also suggested that the hydrogens on the methyl group involved, but not very significantly, in the tunneling coordinates. The predicted inverse $KIE(D_2O)$ by TST and CVT/SCT were almost identical in the entire temperature range. Thus the solvent did not play any significant role in tunneling. The inverse SKIE was caused by the weakening the of hydrogen bonding between the water molecule and the fluoride ion going from the reactants to the TS, as discussed in the previous study.[14] As shown in Table 3, the predicted

Table 3. Calculated KIEs by the TST and CVT/SCT methods

T(K)	KIE(CD_3)		KIE(D_2O)		KIE(^{13}C)		KIE(^{14}C)	
	TST	CVT/SCT	TST	CVT/SCT	TST	CVT/SCT	TST	CVT/SCT
50	0.20	0.39	0.05	0.05	1.34	2.03	1.73	5.60
60	0.28	0.43	0.09	0.09	1.29	2.00	1.60	5.39
70	0.35	0.46	0.13	0.14	1.25	1.96	1.52	5.06
80	0.41	0.49	0.17	0.18	1.22	1.89	1.45	4.63
90	0.47	0.52	0.21	0.22	1.20	1.80	1.40	4.09
100	0.52	0.54	0.24	0.26	1.18	1.69	1.37	3.44
125	0.62	0.62	0.32	0.34	1.15	1.37	1.30	2.05
150	0.69	0.69	0.39	0.40	1.13	1.22	1.25	1.55
175	0.75	0.75	0.45	0.45	1.11	1.16	1.22	1.38
200	0.79	0.79	0.49	0.49	1.10	1.13	1.20	1.30
250	0.85	0.85	0.56	0.56	1.08	1.10	1.16	1.21
300	0.88	0.88	0.61	0.61	1.07	1.08	1.14	1.17
400	0.91	0.92	0.67	0.68	1.06	1.06	1.11	1.13
500	0.93	0.93	0.72	0.72	1.05	1.05	1.09	1.10

$KIE(D_2O)$ decreases as temperature decreases, from 0.61 at 300 K to 0.05 at 100 K. The predicted KIE(^{13}C) and KIE(^{14}C) at higher temperature showed the expected slightly normal KIE which was caused by the bond-breaking between the carbon and the fluorine atoms. For example, the KIE(^{13}C) predicted by TST at 100 K, 200 K, and 300 K were 1.18, 1.10, and 1.07, respectively, while the predicted KIE(^{14}C) were 1.37, 1.20, and 1.14, respectively. One might not expect the carbon atom to show significant tunneling effects even at low temperature due to its much higher mass than the hydrogen atom. However, recent studies showed that in reactions with high barriers and relatively small atom movements, the carbon tunneling could be very significant.[34,35] Indeed, Table 3 showed that the tunneling effects had perceptible effects on carbon KIE below room temperature, and significantly increased the KIE(^{13}C) and KIE(^{14}C) below 150 K. It was quite remarkable that the KIE(^{13}C) and KIE(^{14}C) increased to 2.0 and 5.6 at 50 K. The increase reflected that the motion of carbon atom directly correlated to the reaction path around the transition state. The interesting temperature dependence of the calculated KIEs by the TST and CVT/SCT methods was shown in Figure 4. The familiar KIE(^{13}C) and KIE(^{14}C) values in gas-phase S_N2 reactions obtained in earlier studies only apply to low barrier reactions and at around room temperature. The carbon KIEs calculated in the current study are consistent with results from earlier studies at room temperature. For example, the experimental KIE(^{13}C) of the $F^- + CH_3Cl$, $Br^- + CH_3Cl$, and $CN^- + CH_3Cl$ reactions were measured 1.07, 1.07, and 1.08, respectively, while the calculated values by B3LYP/aug-cc-pVDZ method were 1.06, 1.07 and 1.07, respectively.[36-38] The KIE(^{14}C) of the $OH^- + CH_3I$ and $Ag^- + CH_3I$ reactions were measured 1.08 and 1.09 respectively.[39] The KIE(^{14}C) of 1.13 of the current system at 300 K is slightly higher than those limited experimental data. However, the current study also suggested that for higher-barrier S_N2 reactions the tunneling effects of carbon atoms could be important at lower temperature, which could increase (relative to the TST values) the carbon KIEs significantly, as in the current cases of KIE(^{13}C) and KIE(^{14}C).

SUMMARY

The S_N2 reaction of $F^-(H_2O) + CH_3F$ and four different isotopically substituted analogs have been studied with correlated electronic structure calculations and dual-level dynamics method. The high-level results showed that this reaction has a significant barrier of ~10 kcal/mol. The deuterium (CD_3) and heavy water substituted reactions resulted in inverse KIEs while the ^{13}C and ^{14}C substituted reactions were predicted to show normal KIEs. Despite the reaction involves movement of heavy atoms, our calculation predicted that the tunneling effects would dominate the reactions at temperature below 200 K. The tunneling effects increased the kinetic isotope effects due to the CD_3, ^{13}C, and ^{14}C substitutions at low temperature. Accurate kinetics measurement of the gas-phase high-barrier S_N2 reaction may be beyond the current experimental techniques. However, future experimental tests on the temperature dependence of the KIEs of similar gas-phase S_N2 reaction

would be of great fundamental interest. Furthermore, the current results would have strong implications on the observed isotope fractionation[40,41] in interstellar chemistry at very low temperature.

ACKNOWLEDGMENT

This work is supported by the National Science Council of Taiwan; grant number NSC-100-2113-M-194-007. We are also grateful to the National Center for High-Performance Computing (NCHC) of Taiwan for providing part of the computational resources.

REFERENCES

1. Wladkowski, B. D.; Wilbur, J. L.; Brauman, J. I. *J. Am. Chem. Soc.* **1994**, *116*, 2471.
2. Graul, S. T.; Bowers, M. T. *J. Am. Chem. Soc.* **1994**, *116*, 3875.
3. Cyr, D. M.; Scarton, M. G.; Wiberg, K. B.; Johnson, M. A.; Nonose, S.; Hirokawa, J.; Tanaka, H.; Kondow, T.; Morris, R. A.; Viggiano, A. A. *J. Am. Chem. Soc.* **1995**, *117*, 1828.
4. Gronert, S.; Depuy, C. H.; Bierbaum, V. M. *J. Am. Chem. Soc.* **1991**, *113*, 4009.
5. Meng, Q.; Gogoll, A.; Thibblin, A. *J. Am. Chem. Soc.* **1997**, *119*, 1217.
6. Villano, S. M.; Eyet, N.; Lineberger, W. C.; Bierbaum, V. M. *J. Am. Chem. Soc.* **2009**, *131*, 8227.
7. Garver, J. M.; Fang, Y.-R.; Eyet, N.; Villano, S. M.; Bierbaum, V. M.; Westaway, K. C. *J. Am. Chem. Soc.* **2010**, *132*, 3803.
8. Viggiano, A. A.; Morris, R. A.; Paschkewitz, J. S.; Paulson, J. F. *J. Am. Chem. Soc.* **1992**, *114*, 10477.
9. Boyd, R. J.; Kim, C. K.; Shi, Z.; Weinbergf, N.; Wolfe, S. *J. Am. Chem. Soc.* **1993**, *115*, 10147.
10. O'Hair, R. A. J.; Dang, T. T.; DePuy, C. H.; Bierbaum, V. M. *J. Am.Chem. Soc.* **1994**, *116*, 3609.
11. Hu, W.-P.; Truhlar, D. G. *J. Am. Chem. Soc.* **1995**, *117*, 10726.
12. Hu, W.-P.; Truhlar, D. G. *J. Am. Chem. Soc.* **1996**, *118*, 860.
13. de Koning, L. J.; Nibbering, N. M. M. *J. Am. Chem. Soc.* **1987**, *109*, 1715.
14. Hu, W.-P.; Truhlar, D. G. *J. Am. Chem. Soc.* **1994**, *116*, 7797.
15. Zhao, X. G.; Tucker, S. C.; Truhlar, D. G. *J. Am.Chem. Soc.* **1991**, *113*, 826.
16. Davico, G. E. *J. Phys. Chem. A.* **2006**, *110*, 13112.
17. Viggiano, A. A.; Arnold, S. T.; Morris, R. A.; Ahrens, A. F.; Hierl, P. M. *J. Phys. Chem.* **1996**, *100*, 14397.
18. (a)Truhlar, D. G.; Garrett, B. C. *Acc. Chem. Res.* **1980**, *13*, 440. (b) Truhlar, D. G.; Isaacson, A. D.; Garrett, B. C. In *Theory of Chemical Reaction Dynamics*; Baer, M., Ed.; CRC Press: Boca Raton, FL, 1985; Vol. 4, p 65.
19. Liu, Y.-P.; Lu, D.-H.; Gonzalez-Lafont, A.; Truhlar, D. G.; Garrett, B. C. *J. Am. Chem. Soc.* **1993**, *115*, 7806.
20. (a) Liu, Y.-P.; Lynch, G. C.; Truong, T. N.; Lu, D.-H.; Truhlar, D. G.; Garrett, B. C. *J. Am. Chem. Soc.* **1993**, *115,* 2408. (b) Lu, D.-H.; Truong, T. N.; Melissas, V. S.; Lynch, G. C.; Liu, Y.-P.; Garrett, B. C.; Steckler, R.; Isaacson, A. D.; Rai, S. N.; Hancock, G. C.; Lauderdale, J. G.; Joseph, T.; Truhlar, D. G. *Comput. Phys. Commun.* **1992**, *71*, 235.
21. Truong, T. N.; Lu, D.-H.; Lynch, G. C.; Liu, Y.-P.; Melissas, V. S.; Gonzalez-Lafont, A.; Rai, S. N.; Steckler, R.; Garrett, B. C.; Joseph, T.; Truhlar, D. G. *Comput. Phys. Commun.* **1993**, *75*, 143.
22. Møller, C.; Plesset, M. S. *Phys. Rev.* **1934**, *46* ,618.
23. Stephens, P. J.; Devlin, F. J.; Chabalowski, C. F.; Frisch, M. J. *J. Phys. Chem.* **1994**, *98*, 11623.
24. (a) Dunning, Jr., T. H. *J. Chem. Phys.* **1989**, *90*, 1007. (b) Kendall, R. A.; Dunning, Jr., T. H.; Harrison, R. J. *J. Chem. Phys.* **1992**, *96*, 6796. (c) Woon, D. E.; Dunning, Jr., T. H. *J. Chem. Phys.* **1993**, *98*, 1358.
25. Pople, J. A.; Head-Gordon, M.; Raghavachari, K. *J. Chem. Phys.* **1987**, *87*, 5968.
26. Hu, W.-P.; Liu, Y.-P.; Truhlar, D. G. *J. Chem. Soc. Faraday Trans.* **1994**, *90*, 1715.
27. (a) Page, M.; McIver, J. W., Jr *J. Chem. Phys.* **1988**, *88*, 922. (b) Page, M.; Doubleday, C.; McIver, J. W., Jr *J. Chem. Phys.* **1990**, *93*, 5634.
28. Huang, C.-H.; You, R.-M.; Lian, P.-Y.; Hu, W.-P. *J. Phys. Chem. A* **2000**, *104,* 7200.
29. Gaussian 03, Revision E.01, Frisch, M. J.; Trucks, G. W.; Schlegel, H. B.; Scuseria, G. E.; Robb, M. A.; Cheeseman, J. R.; Montgomery, Jr., J. A.; Vreven, T.; Kudin, K. N.; Burant, J. C.; Millam, J. M.; Iyengar, S. S.; Tomasi, J.; Barone, V.; Mennucci, B.; Cossi, M.; Scalmani, G.; Rega, N.; Petersson, G. A.; Nakatsuji, H.; Hada, M.; Ehara, M.; Toyota, K.; Fukuda, R.; Hasegawa, J.; Ishida, M.; Nakajima, T.; Honda, Y.; Kitao, O.; Nakai, H.; Klene, M.; Li, X.; Knox, J. E.; Hratchian, H. P.; Cross, J. B.; Bakken, V.; Adamo, C.; Jaramillo, J.; Gomperts, R.; Stratmann, R. E.; Yazyev, O.; Austin, A. J.; Cammi, R.; Pomelli, C.; Ochterski, J. W.; Ayala, P. Y.; Morokuma, K.; Voth, G. A.; Salvador, P.; Dannenberg, J. J.; Zakrzewski, V. G.; Dapprich, S.; Daniels, A. D.; Strain, M. C.; Farkas, O.; Malick, D. K.; Rabuck, A. D.; Raghavachari, K.; Foresman, J. B.; Ortiz, J. V.; Cui, Q.; Baboul, A. G.; Clifford, S.; Cioslowski, J.; Stefanov, B. B.; Liu, G.; Liashenko, A.; Piskorz, P.; Komaromi, I.; Martin, R. L.; Fox, D. J.; Keith, T.; Al-Laham, M. A.; Peng, C. Y.; Nanayakkara, A.; Challacombe, M.; Gill, P. M. W.; Johnson, B.; Chen, W.; Wong, M. W.; Gonzalez, C.; Pople, J. A.; Gaussian, Inc.: Wallingford CT, 2004.
30. Corchado, J. C.; Chunag, Y.-Y.; Coitino, E. L.; Truhlar, D. G. *Gaussrate*, version 8.2; University of Minnesota: Minneapolis, MN, 1999.
31. Chuang, Y.-Y.; Corchado, J. C.; Fast, P. L.; Villa, J.; Hu,

W.-P.; Liu, Y.-P.; Lynch, G. C.; Nguyen, K. A.; Jackels, C. F.; Gu, M. Z.; Rossi, I.; Coitino, E. L.; Clayton, S.; Melissas, V. S.; Steckler, R.; Garrett, B. C.; Isaacson, A. D.; Truhlar, D. G. *Polyrate*-version 8.2; University of Minnesota: Minneapolis, MN, 1999.
32. Zhao, Y.; González-García, N.; Truhlar, D. G. *J. Phys. Chem. A* **2005**, *109*, 2012.
33. Zheng, J.; Zhao, Y.; Truhlar, D. G. *J. Chem. Theory Comput.* **2007**, *3*, 569.
34. (a) Albu, T. V.; Lynch, B. J.; Truhlar, D. G.; Goren, A. C.; Hrovat, D. A.; Borden, W. T. ; Moss, R. A. *J. Phys. Chem. A* **2002**, *106*, 5323. (b) Zuev, P. S.; Sheridan, R. S.; Albu, T. V.; Truhlar, D. G.; Hrovat, D. A.; Borden, W. T. *Science* **2003**, *299*, 867. (c) Datta, A.; Hrovat, D. A.; Borden, W. T. *J. Am. Chem. Soc.* **2008**, *130*, 6684. (d) Gonzalez-James, O. M.; Zhang, X.; Datta, A.; Hrovat, D. A.; Borden, W. T.; Singleton, D. A. *J. Am. Chem. Soc.* **2010**, *132*, 12548.
35. (a) Huang, C.-H.; Tsai, L.-C.; Hu, W.-P. *J. Phys. Chem. A* **2001**, *105*, 9945. (b) Fu, Y.-S.; Tsai, S.-C.; Huang, C. H.; Yen, S.-Y.; Hu, W. P.; Yu, S. J. *J. Org. Chem.* **2003**, *68*, 3068.
36. Matsson, O.; Dybala-Defratyka, A.; Rostkowski, M.; Paneth, P.; Westaway, K. C. *J. Org. Chem.* **2005**, *70*, 4022.
37. Lynn, K. R.; Yankwich, P. E. *J. Am. Chem. Soc*. **1961**, *83*, 790.
38. Lynn, K. R.; Yankwich, P. F. *J. Am. Chem. Soc*. **1961**, *83*, 3220.
39. Bender, M. L.; Hoeg, D. F. *J. Am. Chem. Soc.* **1957**, *79*, 5649.
40. Langer, W. D.; Graedel, T. E.; Frerking, M. A.; Armentrout, P. B. *Astrophy* **1984**, *227*, 581.
41. Smith, D. *Chem. Rev.* **1992**, *92*, 1473.

